Supplemental Material for ”Plasmonic enhancement of molecular hydrogen dissociation on metallic magnesium nanoclusters”

Oscar A. Douglas-Gallardo,[1] Connor L. Box,[1] and Reinhard J. Maurer[1, a)]
Department of Chemistry, University of Warwick, Gibbet Hill Road, Coventry, CV4 7AL, UK.

CONTENTS

---

a) Electronic mail: r.maurer@warwick.ac.uk

S1. ELECTRONIC STRUCTURE BENCHMARK CALCULATIONS

The ground-state and time-dependent electronic properties associated with Mg nanoclusters have been computed with the SCC-DFTB method[1] and the 3ob-3-1[2] parameter set. These DFTB parameters were originally parametrised for organic and biological systems, thus its direct transferability to other molecular and metallic systems needs verification. In this context, a set of DFT calculations have been carried out to compare them with the DFTB results, see Figure S1. This validation study shows that DFTB is able to generate reliable results reproducing the general electronic structure features computed at DFT-PBE[3] level. A small error in the lattice constants at the DFTB level is detected for the optimized unit cell (Δc=12.9 and Δa 5.3%).

We have calculated the Mg band structure and Mg density of state (DOS) and compared them with DFTB results. Both properties emerge from the underlying electronic structure and can be used as suitable metric to assess the quality of these parameters. To compute the Mg band structure, a collection of high-symmetry k points on hexagonal closest packed (hcp) structure[4–6] were selected (Γ, M, L, A, K and H).[4] The top panel of Figure S1 shows a very good agreement between the band structure of bulk Mg predicted by DFT and DFTB and both compare fairly well with other reports.[5,6] The band structure at DFT level is characterized by a set of flat bands very close to the Fermi energy (dotted red line) which are quite well described at DFTB level. The energy of the Γ and A points are lower ($<$ -6 eV) at DFT level than the computed ones at DFTB. The band structure at DFT level was computed with the FHI-aims electronic structure package[7] with a k-grid of $16 \times 16 \times 16$, a 'tight' basis set and a lattice constant for metal Mg at PBE level of a=3.19 Å and c=5.12 Å.[8] These values are in good agreement with the experimental values(a =3.21Å and c=5.21 Å).[9] The unit cell employed in the DFTB calculations was first optimized (see inset in bottom panel of Figure S1a for optimized values) using 3ob-3-1 DFTB parameter set. SCF accuracy thresholds employed for the electron density, eigenvalue energies, total energy and force threshold were $1e^{-6}$ e/a_0^3, $1e^{-3}$ eV, $1e^{-6}$ eV and $1e^{-4}$ eV/Å respectively. This good agreement between DFT and DFTB found in the band structure is also extended to the DOS as can be seen in the bottom panels of Figure S1, both show similar profiles and very similar behavior to the free-electron model, which can be assumed for metallic Mg. The DOS was computed by using a denser k-grid ($96 \times 96 \times 96$) considering 4000 points (each 0.01eV) and

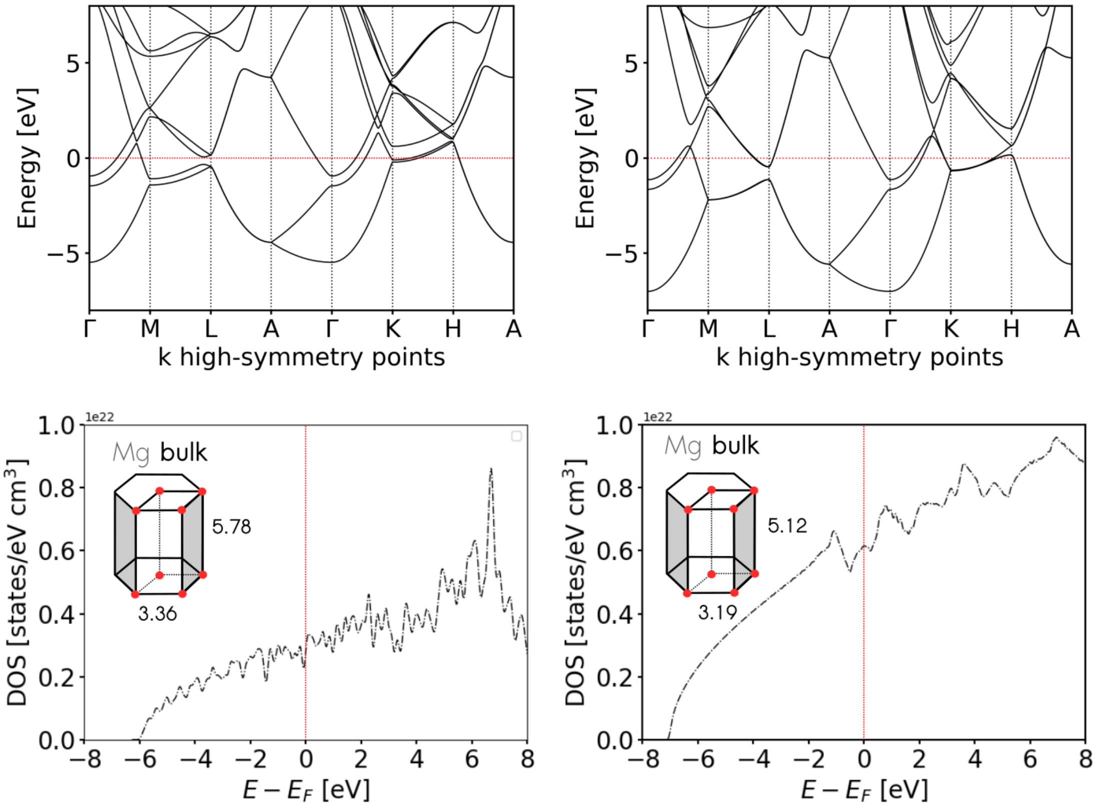

(a) (b)

FIG. S1. Band structure and DOS for Mg bulk computed at (a) DFTB (3ob-3-1) (b) DFT-PBE level of theory. The dotted red lines indicate the Fermi energy in all panels. Inset: Unit cell parameters in Ångstrom obtained after unit cell optimization are shown for Mg hcp crystal structure at DFTB and DFT level. To compute the band structure, a k-grid 16x16x16 was selected. In the case of the DOS a denser k-grid was used (96 × 96 × 96) with a broadening width of 0.05 eV (the same set up was used for DFTB).

with a broadening of 0.05 eV. Both DOS have been normalized by their respective unit cell volume in order to make a fair comparison.

S2. DENSITY OF STATES OF MG NANOCLUSTERS

As part of our validation study, the DOS for a set of small iscosahedral Mg nanoclusters was also computed at DFTB and DFT level, shown in Figure S2. The agreement between DFT and DFTB is generally good, with the general shape and energy range of the DOS

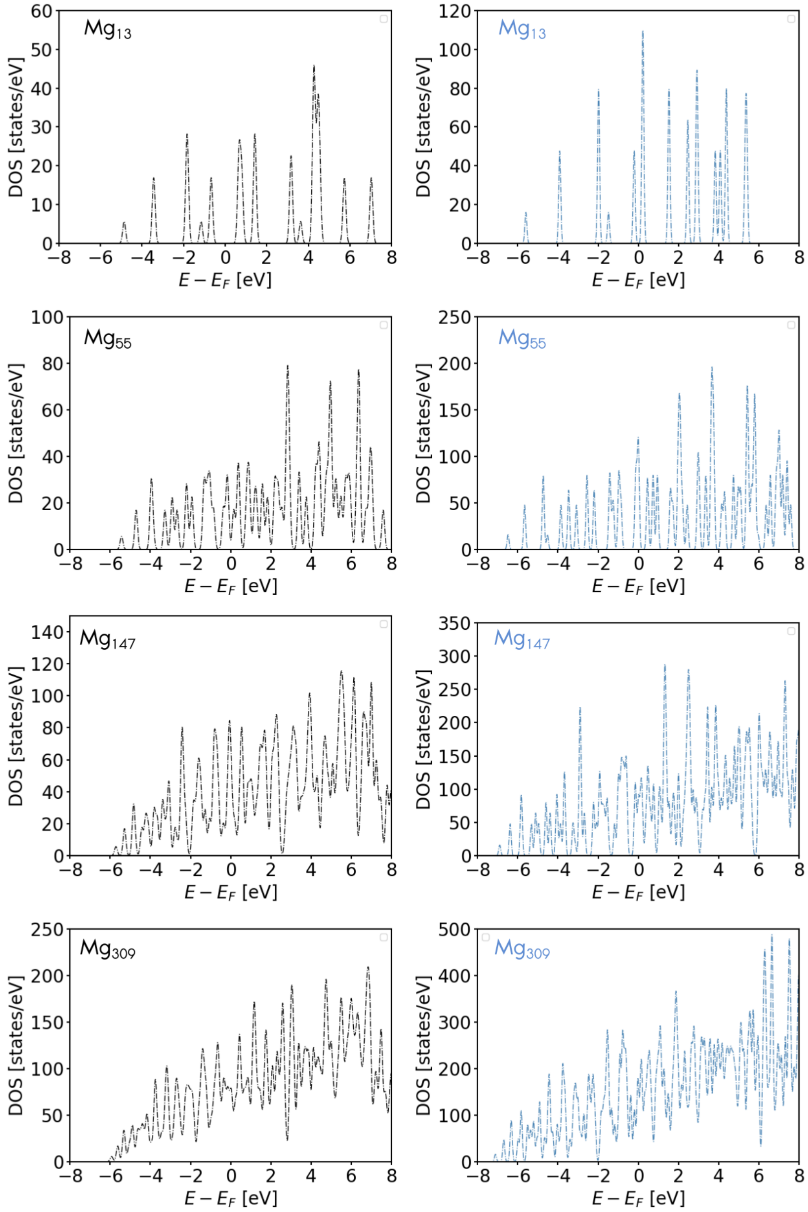

(a) (b)

FIG. S2. DOS for a set of very small Mg nanoclusters containing 13, 55, 147 and 309 metallic atoms computed with (a) DFTB and (b) DFT. The same set up as described in Figure S1 was used to compute the DOS for these systems (but without a k-grid)

captured for a range of particle sizes.

S3. NON-EQUILIBRIUM ELECTRONIC DISTRIBUTIONS

In Figure S3, we fit the non-equilibrium electron distributions calculated with TD-DFTB with a quasi-logarithmic function Φ(E,t)[10,11], for different time steps of the electronic dynamics for both types of external electric fields. The Φ(E,t) is defined as follows:

$$\Phi[E,t] = \Phi[\rho(E,t)] = -\ln[\frac{2}{\rho(E,t)} - 1] \tag{1}$$

where $\rho(E,t)$ is the electronic population distribution at any time t and $\rho(E,0)$=$f(E,0)$ is the Fermi-Dirac distribution at 300 K.

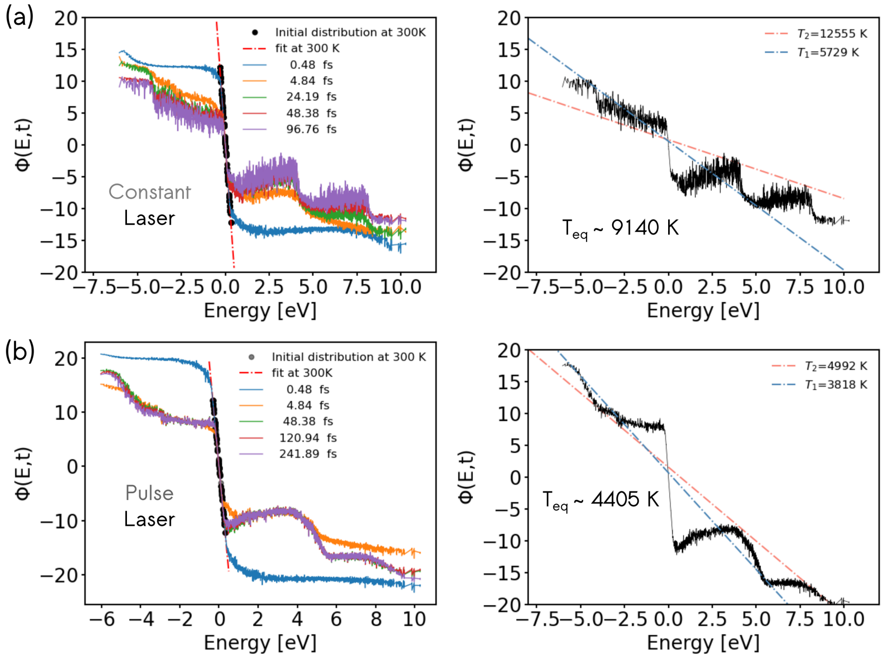

FIG. S3. Quasi-logarithmic representation of non-equilibrium distribution computed at different steps of the electronic dynamics for both (a) constant and (b) pulsed laser sources for the 1415 atom Mg nanocluster. The right panels further show a rough estimation of the electronic temperature by performing a linear fit to a Fermi-Dirac distribution. The blue dash-dotted lines correspond to fits with minimal residuals. The red dash-dotted fits correspond to fits on the extrem step edges of the distribution. This is to better estimate the variance of electronic temperatures in this approximate approach that stems from the fact that the system is not indeed in electronic equilibrium.

For both external electric fields the initial distribution at 300 K is shown with black dots. This initial distribution can be very well described by a Fermi-Dirac distribution function at 300 K (dotted red lines) in this quasi-logarithmic representation. Also, a rough electronic temperature estimation was calculated for both laser sources by computing the slope associated with the external edge of the stepwise structure (see right panels) at 96.76 fs and 241.89 fs, respectively. The obtained final electronic temperatures associated with the equilibrium state (after electron-electron thermalization) turned out to be $\sim 9142 \pm 3413$ K and $\sim 4405 \pm 587$ K for constant and pulsed laser sources, respectively.

S4. HOT-CARRIER DISTRIBUTION FOR DIFFERENT MG NANOCLUSTER SIZES

The hot-carrier distribution generation process was also computed for Mg nanoclusters of different sizes. Figure S4 shows the hot-carrier distribution computed after 96.76 fs when a constant laser source is used as external electric field with a field intensity of $E_0 = 0.02\ V\ \AA^{-1}$.

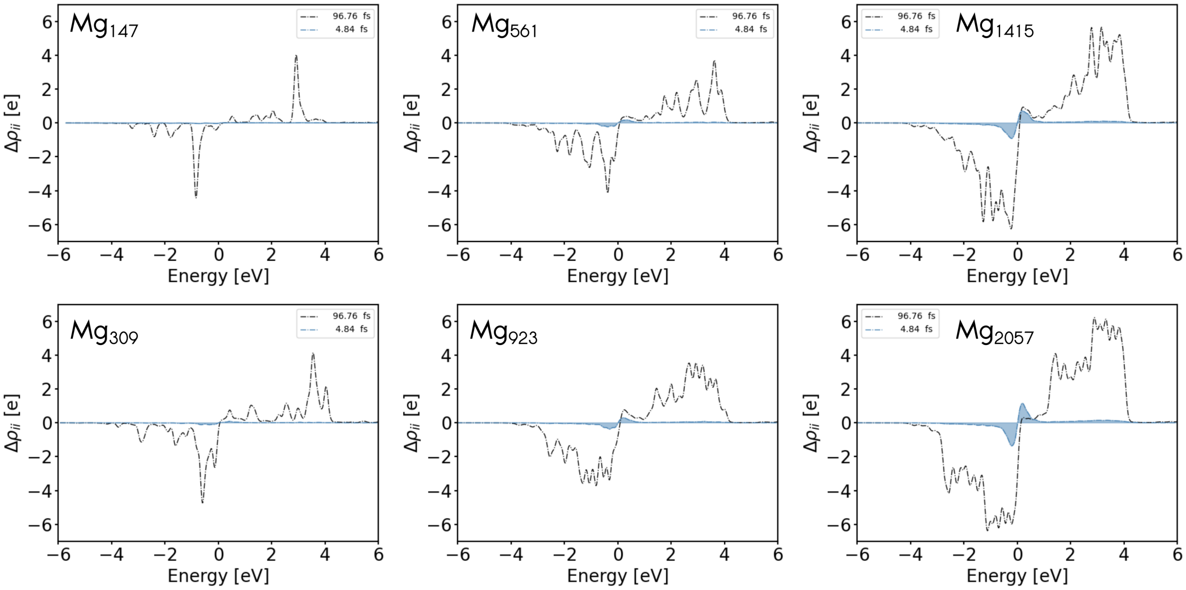

FIG. S4. Evolution of molecular orbitals (MO) population $\Delta\rho_{ii}$ for different particle sizes at 4.84 and 96.76 fs of electronic dynamic by using a constant laser source with an electric field intensity at 0.02 V $\AA^{-1}$.

S5. COMPARISON OF MG AND AG PLASMONIC RESPONSE; DIPOLE MOMENT

The dipole moment signal was used to extract the linewidth and lifetime associated with plasmonic excitation for both plasmonic metals. Figure S5 shows the dipole moment obtained from our electronic dynamics simulation under constant laser source.

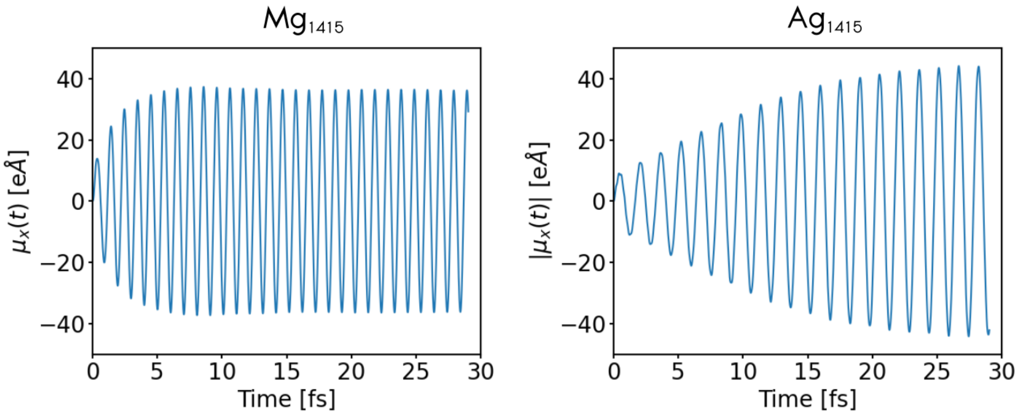

FIG. S5. Dipole moment (x-component) obtained from electronic dynamics driven by a constant laser source with a frequency in tune with the plasmonic excitation for a Mg (ω_{LSPR}= 4.069 eV) and Ag (ω_{LSPR}= 2.7098 eV) nanocluster with 1415 metallic atoms. In both cases an electric field intensity of E_0=0.02 V $\AA^{-1}$ was used.

S6. COMPARISON OF MG AND AG PLASMONIC RESPONSE; HOT-CARRIERS

Also, the hot-carriers energetic landscape produced for a Mg nanocluster was computed and compared with the hot-carrier profile generated by a similar Ag nanocluster. Figure S6 shows the raw hot-carrier energetic landscape (without normalization by DOS as done in the main manuscript) obtained from our electronic dynamic simulation at 43.54 fs under constant laser source for both metals.

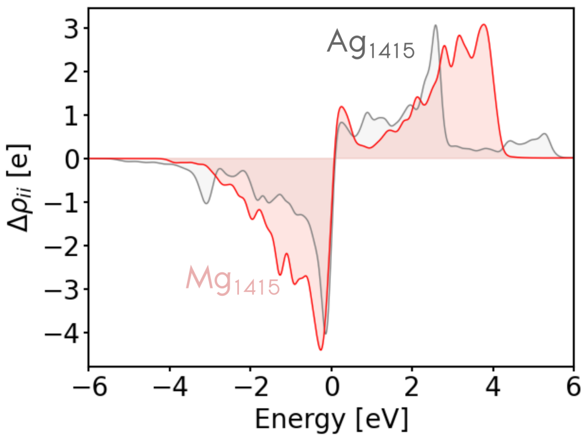

FIG. S6. The hot-carrier distribution computed for a Ag and Mg nanoclusters with 1415 metallic atoms at 43.54 fs. In both cases a constant laser source with an electric field intensity of E_0=0.02 V Å^{-1} was used.

S7. MINIMUM ENERGY PATH AND NONADIABATIC RELAXATION RATES FOR A PERIODIC MG(0001) SLAB

The hydrogen dissociation reaction was also explored on a periodic Mg(0001) slab. For this system the minimum energy path (MEP) was computed by using the climbing-image nudged elastic band (CI-NEB) method implemented in ASE and FHI-aims.[12,13] The reaction and activation energies computed at PBE level were -0.02 eV and 0.89 eV, respectively. Likewise, in order to characterize the non-adiabatic effects associated with this chemical reaction, the relaxation rates due to electronic friction were also computed along this reactive path. For each geometry we use first order time-dependent perturbation theory on the Kohn-Sham DFT wavefunctions to calculate the rate of energy loss for each coordinate due to coupling with hot electrons.[14] We use a broadening of the electronic states of 0.6 eV, a Fermi factor corresponding to an electronic temperature of 300 K and a 'tight' basis set. SCF accuracy thresholds employed for the electron density, eigenvalue energies and total energy were 1e^{-6} e/a$_0^3$, 1e^{-3} eV and 1e^{-6} eV respectively. The details of this procedure are explained in Ref. 14 The Figure S8a and S8b show the obtained MEP and the resulting electronic friction relaxation rates for this system. Figures S8c and S8d show the convergence tests for different k-grids at two special points, the TS and FS. This test shows that k-grid 12 × 12 × 1 is a robust value to compute the electron friction elements for this periodic system.

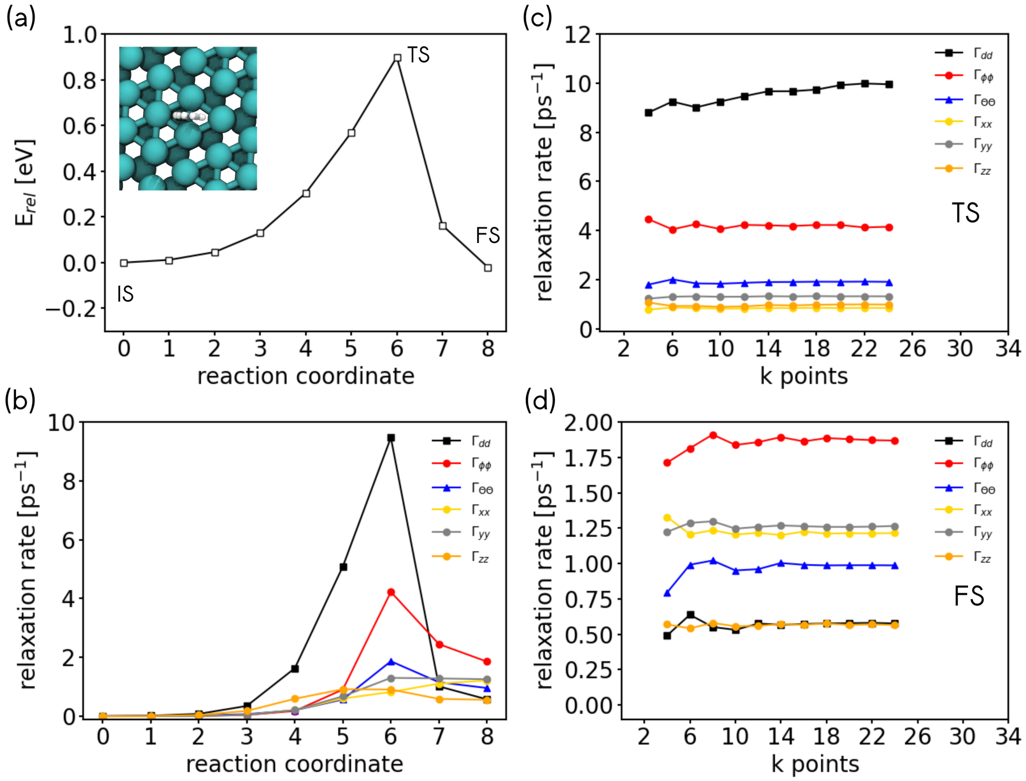

FIG. S7. (a) Minimum energy path (MEP) and (b) electronic friction relaxation rates associated with the hydrogen dissociation reaction on a periodic Mg(0001) slab. Initial state, transition state, and final chemisorbed state are abbreviated as IS, TS, and FS, respectively. The panels (c) and (d) show the diagonal elements of the electron friction tensor transformed into molecular internal coordinates for different k-grid values obtained for the transition state (TS) and final state (FS), respectively. The defintion of internal coordinates is given in Ref. 15.

S8. PROJECTED DOS ALONG MINIMUM ENERGY PATH

In order to gain insights into the hydrogen dissociation/recombination reaction, the projected density of states (pDOS) over hydrogen atomic orbitals (AOs) was computed for three different states along the MEP (IS, TS, and FS) for both model systems, for a small Mg nanocluster with 55 metallic atoms and a periodic Mg(0001) slab. Figure S8 shows the pDOS over hydrogen MOs for both systems.

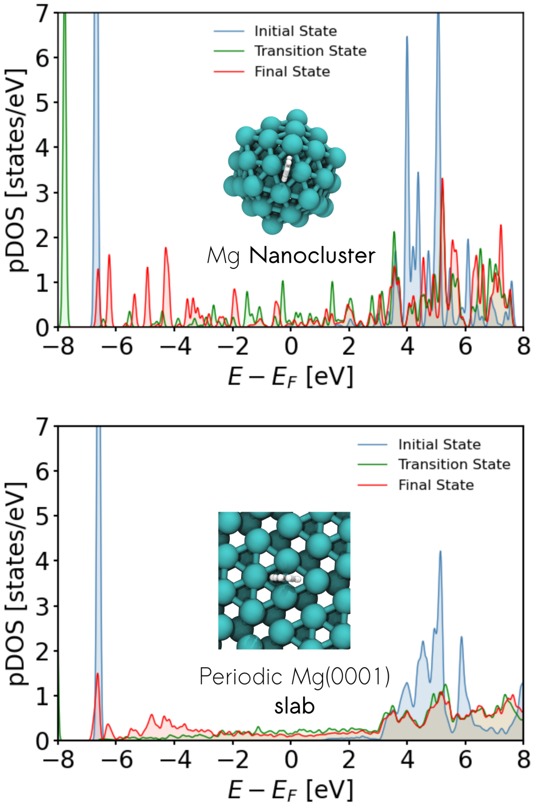

FIG. S8. Projected density of state (pDOS) for hydrogen atomic orbitals along the MEP computed for the small Mg nanocluster (top panel) and the periodic Mg(0001) metallic slab at three different states (IS, TS and FS). The pDOS was computed at PBE level by using a similar set up as shown in Figure S1.

S9. TWO-TEMPERATURE MODEL

To describe the electronic (T_{el}) and phonon (T_{ph}) temperature evolution under ultra-fast laser excitation on a Mg surface, the two temperature model (TTM)[16] was employed. The temporal evolution of both temperatures is described by means of two coupled thermal diffusion equations which in their simplest version (1D-TTM) are:

$$C_{el}\frac{\partial T_{el}}{\partial t} = \frac{\partial \kappa_{el}}{\partial z}\frac{\partial T_{el}}{\partial z} - G_0(T_{el} - T_{ph}) + S(z,t) \tag{2}$$

$$C_{ph}\frac{\partial T_{ph}}{\partial t} = G_0(T_{el} - T_{ph}) \tag{3}$$

Here, C$_{el}$ and C$_{ph}$ are electron and phonon heat capacities, G_0 is the *effective electron-phonon-coupling constant* and κ_{el} is the electronic heat conductivity. A linear temperature dependence for the electronic heat capacity ($C_{el} = \gamma_{el}T_{el}$) and electronic heat conductivity ($\kappa_{el} = \kappa_{RT}(T_{el}/T_{ph})$) was assumed. $S(z,t)$ is the laser source term and z is the vertical position within the metal relative to the surface ($z = 0$). A Gaussian function has been selected to describe the laser source term.

The *effective electron-phonon coupling constant* (G_0) can be related with the electron-phonon coupling constant(λ) with following equation,[17]

$$G_0 = \frac{1}{V_c}(\frac{\pi k_B}{\hbar}) \times \lambda\langle\omega^2\rangle \times g(\epsilon_F) \tag{4}$$

where, V_c is the volume of the unit cell, k_B is the Boltzmann's constant, $\hbar$ is the reduced Plack's constant and $g(\epsilon_F)$ is the electronic DOS at the Fermi level. Here, V_c and $g(\epsilon_F)$ values were determined by using our calculated values at PBE level.[8] To compute the G_0 from the λ=0.28 value,[18] the following approximation was used $\langle\omega^2\rangle \approx \theta_D^2/2$.[18,19] Here, θ_D is the Debye temperature for Mg. The final computed value is $G_0 = 6.75 \times 10^{16}$ W K^{-1} m^{-3}. The other used thermophysical properties were, γ_{el} = 71.00 J m^{-3} K^{-2} (electron specific heat constant), κ_{RT} = 156.00 W m^{-1} K^{-1} (thermal conductivity at 300K), θ_D = 400 K (Debye Temperature).[20] For the laser source, a Gaussian form was selected similar to Ref. 21 (FWHM = 150 nm and $\tau = \frac{FWHM}{2\sqrt{2ln2}}$ and optical penetration depth ζ = 8.96 nm)

S10. LASER-DRIVEN HEATING OF HYDROGEN ATOMS ON MG

We estimate the kinetic energy that can be transferred via hot electrons into chemisorbed hydrogen atoms by propagating an Ornstein-Uhlenbeck process for each of the three degrees of freedom of the atom:[22]

$$dv = -\gamma v dt + \sqrt{k_B T M^{-1} 2\gamma} dW \tag{5}$$

The first term on the right hand side corresponds to the friction contribution and the second term to the random force that describes energy transfer from the bath of hot electrons to the adsorbate. γ is the friction coefficient, T is the electronic temperature, and dW is a random Wiener process.

According to the relaxation rates we find in Figure 5 of the main manuscript, we assume a friction coefficient that corresponds to a relaxation rate of 2 ps^{-1}. The three temperature profiles calculated with the TTM and shown in the inset of Figure 5 of the main manuscript are used to drive the time-dependent electronic temperature in eq. 5. They correspond to laser fluences of 10, 50, and 100 $\mathrm{J/m^2}$ leading to peak electronic temperatures of 2500, 5500, and 8000 K, respectively. For each condition, we simulate 1000 trajectories and calculate the average kinetic energy of hydrogen at 250 fs after $t = 0$ of the laser pulse. For 10, 50, and 100 $\mathrm{J/m^2}$, we find a kinetic energy of the H atom of 0.17, 0.40, and 0.55 eV.

S11. FULL-OPTIMIZATION EFFECT ON MG PLASMONIC RESPONSE

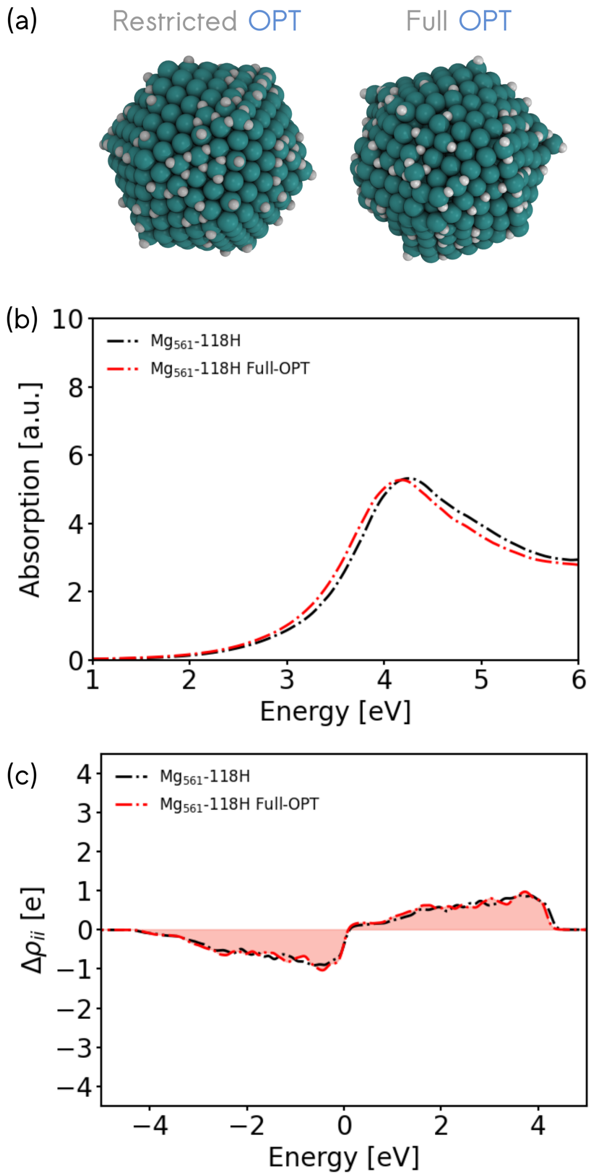

FIG. S11. (a) Optimized structures for a Mg nanocluster with 118 H atoms with and without surface relaxation. (b) Optical absorption response and (c) hot-carrier distribution for both structures consider in (a). The electric field intensity used to produce the hot-carrier distribution in both configuration was E_0=0.02 V $\AA^{-1}$. In this figure, "OPT" is referring to structural optimization.

The full optimization process generates a local surface relaxation on the Mg metal surface which has only minor effects on the optical absorption properties and hot-carrier distribution.

The potential effects associated with the plasmonic response may be harnessed while the plasmonic properties and metallic character are held which is what is expected to happen during the early hydrogen adsorption stage.

REFERENCES

[1] B. Aradi, B. Hourahine, and T. Frauenheim, J. Phys. Chem. A **111**, 5678 (2007).

[2] X. Lu, M. Gaus, M. Elstner, and Q. Cui, J. Phys. Chem. B **119**, 1062 (2015), pMID: 25178644.

[3] J. P. Perdew, K. Burke, and M. Ernzerhof, Phys. Rev. Lett. **77**, 3865 (1996).

[4] W. Setyawan and S. Curtarolo, Comput. Mate. Sci. **49**, 299 (2010).

[5] L. M. Falicov and A. B. Pippard, Philos. Trans. R. Soc. A **255**, 55 (1962).

[6] A. Leonardo, I. Y. Sklyadneva, V. M. Silkin, P. M. Echenique, and E. V. Chulkov, Phys. Rev. B **76**, 035404 (2007).

[7] V. Blum, R. Gehrke, F. Hanke, P. Havu, V. Havu, X. Ren, K. Reuter, and M. Scheffler, Comput. Phys. Commun. **180**, 2175 (2009).

[8] U. Wedig, M. Jansen, B. Paulus, K. Rosciszewski, and P. Sony, Phys. Rev. B **75**, 205123 (2007).

[9] L. J. Slutsky and C. W. Garland, Phys. Rev. **107**, 972 (1957).

[10] B. Y. Mueller and B. Rethfeld, Phys. Rev. B **87**, 035139 (2013).

[11] S. Weber and B. Rethfeld, Appl. Surf. Sci. **417**, 64 (2017), 10th International Conference on Photoexcited Processes and Applications.

[12] G. Henkelman, B. P. Uberuaga, and H. Jónsson, The Journal of Chemical Physics **113**, 9901 (2000).

[13] A. H. Larsen, J. J. Mortensen, J. Blomqvist, I. E. Castelli, R. Christensen, M. Dułak, J. Friis, M. N. Groves, B. Hammer, C. Hargus, E. D. Hermes, P. C. Jennings, P. B. Jensen, J. Kermode, J. R. Kitchin, E. L. Kolsbjerg, J. Kubal, K. Kaasbjerg, S. Lysgaard, J. B. Maronsson, T. Maxson, T. Olsen, L. Pastewka, A. Peterson, C. Rostgaard, J. Schiøtz, O. Schütt, M. Strange, K. S. Thygesen, T. Vegge, L. Vilhelmsen, M. Walter, Z. Zeng, and K. W. Jacobsen, J. Phys.Condens. Matter **29**, 273002 (2017).

[14] R. J. Maurer, M. Askerka, V. S. Batista, and J. C. Tully, Phys. Rev. B **94**, 115432 (2016).

[15] C. L. Box, Y. Zhang, R. Yin, B. Jiang, and R. J. Maurer, JACS Au **1**, 164 (2021).

[16] S. I. Anisimov, B. L. Kapeliovich, and T. L. Perel'man, J. Exp. Theor. Phys. **66**, 776 (1974).

[17] S. L. Daraszewicz, Y. Giret, H. Tanimura, D. M. Duffy, A. L. Shluger, and K. Tanimura, Appl. Phys. Lett. **105**, 023112 (2014).

[18] A. Leonardo, I. Sklyadneva, P. Echenique, and E. Chulkov, Surf. Sci. **601**, 4018 (2007).

[19] Z. Lin, L. V. Zhigilei, and V. Celli, Phys. Rev. B **77**, 075133 (2008).

[20] C. Kittel, Introduction to Solid State Physics (Wiley, 2004).

[21] R. Scholz, S. Lindner, I. Lončarić, J. C. Tremblay, J. I. Juaristi, M. Alducin, and P. Saalfrank, Phys. Rev. B **100**, 245431 (2019).

[22] B. Leimkuhler and C. Matthews, J. Chem. Phys. **138**, 174102 (2013).